On the Adaptivity of Unscented Particle Filter for GNSS/INS Tightly-Integrated Navigation Unit in Urban Environment

IEEE Access
Multidisciplinary ⋮ Rapid Review ⋮ Open Access Journal

Received September 30, 2021, accepted October 17, 2021, date of publication October 21, 2021, date of current version October 28, 2021.

Digital Object Identifier 10.1109/ACCESS.2021.3122006

On the Adaptivity of Unscented Particle Filter for GNSS/INS Tightly-Integrated Navigation Unit in Urban Environment

OLIVIERO VOUCH[1], (Member, IEEE), ALEX MINETTO[1], (Member, IEEE), GIANLUCA FALCO[2], AND FABIO DOVIS[1], (Member, IEEE)

[1]Department of Electronics and Telecommunications (DET), Politecnico di Torino, 10129 Turin, Italy
[2]Space and Navigation Technologies Area, LINKS Foundation, 10138 Turin, Italy

Corresponding author: Oliviero Vouch (oliviero.vouch@polito.it)

ABSTRACT Tight integration algorithms fusing Global Navigation Satellite System (GNSS) and Inertial Navigation System (INS) have become popular in many high-accuracy positioning and navigation applications. Despite their reliability, common integration architectures can still run into accuracy drops under challenging navigation settings. The growing computational power of low-cost, embedded systems has allowed for the exploitation of several advanced Bayesian state estimation algorithms, such as the Particle Filter (PF) and its hybrid variants, e.g. Unscented Particle Filter (UPF). Although sophisticated, these architectures are not immune from multipath scattering and Non-Line-of-Sight (NLOS) signal receptions, which frequently corrupt satellite measurements and jeopardise GNSS/INS solutions. Hence, a certain level of modelling adaptivity should be granted to avoid severe drifts in the estimated states. Given these premises, the paper presents a novel Adaptive Unscented Particle Filter (AUPF) architecture leveraging two cascading stages to cope with disruptive, biased GNSS input observables in harsh conditions. A INS-based signal processing block is implemented upstream of a Redundant Measurement Noise Covariance Estimation (RMNCE) stage to strengthen the adaptation of observables' statistics and improve the state estimation. An experimental assessment is provided for the proposed robust AUPF that demonstrates a 10 % average reduction of the horizontal position error above the 75-th percentile. In addition, a comparative analysis both with previous adaptive architectures and a plain UPF is carried out to highlight the improved performance of the proposed methodology.

INDEX TERMS Bayes methods, sensor fusion, inertial navigation, satellite navigation systems, particle filters, adaptive estimation, position accuracy.

I. INTRODUCTION

Over recent years, the demand for reliable and robust localisation capabilities has become increasingly urgent in critical application domains, such as autonomous driving for land-vehicles or unmanned flight for drones. Scaling down to urban navigation (e.g., a city downtown), Global Navigation Satellite System (GNSS)-only Positioning, Navigation and Timing (PNT) cannot meet strict accuracy, reliability and continuity requirements, although it still sets as the leading technology for absolute positioning in outdoor applications. In fact, street canyons identify challenging scenarios characterised by impairing phenomena such as signal blockages, poor satellite geometry and multipath [1]–[3], which detrimentally affect the quality of Position, Velocity, Timing (PVT) solutions [4]. In such framework, strong research effort has been put to overcome performance limitations of standalone GNSS through the integration of additional positioning information and exploiting advanced signal processing strategies. Among the options, coupling a GNSS receiver to Inertial Navigation Systems (INSs) is a common choice in many mass-market navigation units, thanks to the availability of small and low-cost Inertial Measurement Units (IMUs) in the consumer segment (e.g., micro electro-mechanical sensors [5]). While the good long-term stability of GNSS is helpful to initialise and update the inertial navigation solution

The associate editor coordinating the review of this manuscript and approving it for publication was Wentao Fan.

and prevent it from drifting, the short-term accuracy and the high resolution of a INS allow to finely track the motion dynamics and to aid the solution in presence of GNSS system outages [6], [7].

Different architectural paradigms exist for GNSS/INS integration, which can be broadly summarized in three classes: loose coupling [8], [9], tight coupling [10] and ultra-tight coupling [11], [12]. Although traditionally implemented for professional high-grade IMUs only, positioning units based on a tight integration of low-cost sensors have shown performance improvements for urban settings [9], [10], [13].

The growing availability of high-performance embedded processors at sustainable costs has paved the way to high complexity Monte-Carlo (MC) Bayesian filters, such as Particle Filters (PFs) [14], which represent efficient simulation-based techniques to pursue optimal state estimation [15], [16]. Besides handling non-Gaussian filtering models, they manage to accommodate multiple analytic densities to characteris e measurement noise statistics [17]. Different works [18]–[20] have considered the use of PFs in low-cost GNSS/INS systems for high-accuracy positioning and navigation in land-vehicle applications. Among them, a hybrid PF-based implementation - the Unscented Particle Filter (UPF) [21], [22] - targets to improve the Importance Sampling (IS) process by operating an upstream Unscented Kalman Filter (UKF) [23], [24]. The latter is meant to deliver an accurate enough approximation of the optimal importance density, matching with the posterior state density, to feed the underlying PF stage.

However sophisticated the estimation process is, the optimality of the filtering algorithm is strongly driven by the accuracy on the statistical characterisation of measurements noise components. Such stochastic terms are modelled via the observation covariance matrix which leverages the a-priori stochastic knowledge available in the navigation filter. In fact, tight GNSS/INS units exploit the measurement model in the filter correction step to update the description of motion dynamics and refine the state prediction though input GNSS data; hence, the noise terms affecting GNSS observables are fundamental as they embed information about unmodelled error sources as well. In real-time kinematic applications, uncertainties in the dynamic environment jeopardise the estimation quality of measurement noise covariance and lead to sub-optimal, or even divergent, navigation solutions. In this sense, deep urban settings are challenging because highly-corrupted satellite signals can induce misleading biases on input observables and reduce the predictability of their statistics. Therefore, it is necessary to make full use of the information collected along the filtering process to achieve higher immunity of the state estimation from accidental disturbances [25].

In such framework, semi-static Bayesian formulations, like the one proposed in [26], build on functional relationships with satellite measurements and leverage parameter estimation to construct a covariance estimate. Unfortunately, they leak promptness in triggering environmental changes and mirroring them on error statistics. Hence, they struggle to inhibit signal outliers from spoiling the state estimation and undermining the integrity of the navigation solution. Conversely, adaptive estimation formulations leverage the learning ability of the navigation filter, based on a buffer of input GNSS data bringing innovation, to dynamically update the a-priori statistical information and tune the observations' covariance model accordingly. By far, Innovation-based Adaptive Estimation (IAE) and Residual-based Adaptive Estimation (RAE) identify the most popular strategies to pursue dynamic measurement noise estimation in the GNSS/INS framework, leading to the definition of an Adaptive Unscented Particle Filter (AUPF) scheme [27]–[29].

However, these methods leverage a variance model which indirectly depends on the state vector estimate; as such, any bias in the navigation solution can potentially spread over stochastic noise characterisation. Furthermore, traditional adaptive implementations do not support any pre-filtering of input GNSS observables. Hence, they are still vulnerable to biasing phenomena affecting input GNSS ranging measurements and the problem of filter divergence in signal-deteriorated scenarios is still unsolved.

Based on these premises, this paper presents a novel tight architecture for an error-based GNSS/INS unit exploiting an AUPF with embedded countermeasures to grant improved robustness in harsh navigation context with remarkable signal degradation. Specifically, the canonical UPF architecture is augmented with a cascaded, double-stage adaptive module including the following items:

- a INS-based pre-processing stage to reduce instability against unpredictable (e.g., multipath-related) bias injections affecting input GNSS ranging measurements.
- an adaptive, state-free measurement error covariance estimation stage - namely, Redundant Measurement Noise Covariance Estimation (RMNCE) - exploiting pre-processed GNSS measurements to better predict the navigated environment.

The proposed solution is experimentally assessed to explore the impact of adaptivity on a hybrid UPF estimator, and to investigate the AUPF positioning accuracy against a plain UPF approach. To this end, the following analysis employs a real dataset about a car-ride along a urban trajectory.

The paper outline is organized as follows: Section II recalls the fundamentals about GNSS/INS integration with the mathematical formalization of a filtering system model in indirect configuration, and overviews the UPF Bayesian architecture in a nutshell. Section III, then, presents the adaptive model optimizations to enhance the UPF positioning accuracy and estimation robustness under highly-degraded signal environments. Eventually, Section IV discusses the experimental outcomes from the assessment in urban scenario and specifies the simulation setup as well as the adopted methodology.

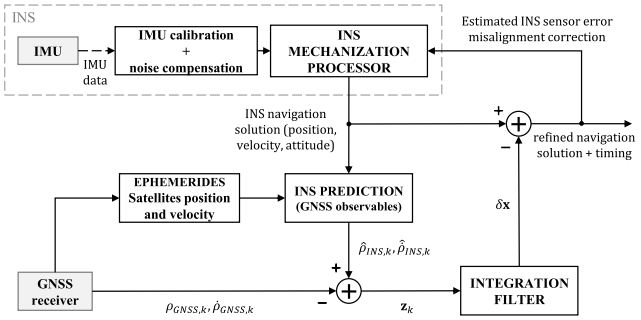

FIGURE 1. Block-diagram of GNSS/INS tightly-coupled architecture.

II. GNSS/INS TIGHT INTEGRATION WITH UNSCENTED PARTICLE FILTER: OVERVIEW AND FUNDAMENTALS

A. THE INTEGRATED ARCHITECTURE AT A GLANCE

A conventional GNSS/INS tightly integrated unit implements a centralised filtering scheme, where the raw data generated by both INS and GNSS are fused to generate a single, blended navigation solution [30]. More in depth, raw GNSS measurements - namely, pseudorange and Doppler-shift - are streamed to an integration processor which mechanises a high-order integration filter and aids the position, velocity and attitude high-rate updates from the INS [31], [32]. Employing raw measurements, tight integration is more robust under any GNSS outages and the navigation system performance improves in degraded signal environments [33]. In fact, INS sensors (i.e., accelerometers and gyroscopes) can be calibrated in real-time to improve standalone inertial performance in absence of tracked GNSS satellites. Furthermore, INS outputs can be exploited to tighten GNSS Doppler tracking loops, and the position estimates from the INS can be used for faster re-acquisition after GNSS outages [32].

Fig. 1 shows a simplified block-scheme for a tight GNSS/INS integration. The inertial system acts as a self-contained processing unit, the *INS mechanisation processor*, dead-reckoning position, velocity and attitude data from the high-rate measurements supplied by IMU sensors. In addition, the INS predicts nominal pseudorange and pseudorange-rate trends related to the set of tracked GNSS satellites. Meanwhile, the GNSS receiver supplies raw pseudorange and Doppler-shift measurements that constitute the navigational aid allowing the *integration filter* to update the INS navigation solution. Eventually, the refined solution is used as the output of the whole integrated unit [9], [10], [34].

B. ERROR-BASED GNSS/INS SYSTEM MODEL

The rigorous formulation of a state-space model for the system under analysis is pivotal to the development of an integration algorithm fusing data from heterogeneous sources. It includes the definition of both process and measurement dynamics combined with a convenient modelling of their error statistics. These models must be faithful enough to adequately represent the system evolution, but functional as well to foster the development of the integration routine [35], [36].

In GNSS/INS integrated units, the estimated states include navigation parameters (i.e., position, velocity, attitude), sensor parameters (i.e., biases and scale factors) and timing parameters (i.e., clock bias and drift) [37]. Pursuing an indirect navigation model formulation, the integration filter relies on the propagation equation of inertial errors; as such, it estimates navigation errors and inertial sensor errors useful to correct earlier predictions from the INS-only navigation solution [38]. In the following, the symbol δ will indicate a correction to the quantity it is prepended to.

In the framework of a GNSS/INS tight architecture, the navigation error state vector can be defined as follows [10]:

$$\boldsymbol{\delta x}^{e}_{17\times1} = \left[\boldsymbol{\delta r}^{e}_{3\times1}\ \boldsymbol{\delta v}^{e}_{3\times1}\ \boldsymbol{\epsilon}^{e}_{3\times1}\ \boldsymbol{\delta b}^{b}_{a,3\times1}\ \boldsymbol{\delta b}^{b}_{g,3\times1}\ \boldsymbol{\delta t}_{u,2\times1}\right]^{T} \quad (1)$$

where superscripts e and b refer to Earth-Centred Earth-Fixed (ECEF) frame and local body frame, respectively. From (1) we can identify the following terms:

- $\boldsymbol{\delta r}^{e}_{3\times1} = \left[\delta r^{e}_{x}\ \delta r^{e}_{y}\ \delta r^{e}_{z}\right]^{T}$ is the position error vector along the three Cartesian axes of the ECEF frame;
- $\boldsymbol{\delta v}^{e}_{3\times1} = \left[\delta v^{e}_{x}\ \delta v^{e}_{y}\ \delta v^{e}_{z}\right]^{T}$ is the velocity error vector along the three Cartesian axes of the ECEF frame;
- $\boldsymbol{\epsilon}^{e}_{3\times1} = \left[\epsilon^{e}_{x}\ \epsilon^{e}_{y}\ \epsilon^{e}_{z}\right]^{T}$ is the vector of IMU axes misalignment angles (i.e., attitude errors), expressed in ECEF coordinates;
- $\boldsymbol{\delta b}^{b}_{a,3\times1} = \left[\delta b^{b}_{a,x}\ \delta b^{b}_{a,y}\ \delta b^{b}_{a,z}\right]^{T}$ is the error vector associated to specific force measurements (from accelerometers) along the triaxial body frame reference;
- $\boldsymbol{\delta b}^{b}_{g,3\times1} = \left[\delta b^{b}_{g,x}\ \delta b^{b}_{g,y}\ \delta b^{b}_{g,z}\right]^{T}$ is the error vector associated to angular rate measurements (from gyroscopes) along the triaxial body frame reference;
- $\boldsymbol{\delta t}_{u,2\times1} = \left[\delta t_{u}\ \delta \dot{t}_{u}\right]^{T}$ is the vector collecting the estimated clock bias and clock drift;

The next step in the state-space formulation requires the definition of a INS error model meant to describe the dynamics of both navigation and sensor error states in (1). The derivation of a mechanisation involving inertial error propagation equations leverages a perturbation of the non-linear inertial navigation equations [39], and results in matrix equation (2), as shown at the bottom of the next page, [10]; the following terms are identified:

- $\mathbf{F}^{e}_{3\times3}$ is the skew-symmetric form of accelerometer measurements, expressed in the ECEF frame;
- $\mathbf{N}^{e}_{3\times3}$ is the tensor form of the gradient operator applied to the gravity vector $\boldsymbol{g}$, expressed in the ECEF frame;
- $\boldsymbol{\delta f}^{b}_{3\times1}$ collects the body frame triaxial error components on accelerometer measurements;
- $\boldsymbol{\delta \omega}^{b}_{ib,3\times1}$ collects the body frame triaxial error components on gyroscope measurements;

The linearized error mechanisation model (2) would fit with the error states dynamics for a GNSS/INS system only in case the inertial sensor error vectors - specifically, $\boldsymbol{\delta f}^{b}_{3\times1}$ and $\boldsymbol{\delta \omega}^{b}_{ib,3\times1}$ - agreed with a zero-mean, multivariate normal distribution. Unfortunately, these conditions do not apply due

to the presence of deterministic sensor bias components that move the average of the error distribution [10]. A rigorous INS error model is formalised in [39] and, starting from it, [10] proposes a simpler but effective additive error model (first-order linearization) for IMU sensors measurements:

$$\begin{aligned} \delta \boldsymbol{f}^b &= \boldsymbol{b}_a + \boldsymbol{\omega}_f \\ \delta \boldsymbol{\omega}_{ib}^b &= \boldsymbol{b}_g + \boldsymbol{\omega}_\omega \end{aligned} \tag{3}$$

where the error of each sensor includes two components:

- $\boldsymbol{b}_a$ and $\boldsymbol{b}_g$ are the bias drifts related to accelerometers and gyroscopes, respectively;
- $\boldsymbol{\omega}_f$ and $\boldsymbol{\omega}_\omega$ are additive noise components affecting accelerometers and gyroscopes, respectively.

The bias terms embody theoretical time-dependent effects (e.g., temperature sensitivity, scale factors etc. [10]) neglected in the reduced model.

Incorporating sensor error model (3), the resulting continuous-time INS error mechanisation suitable for a tight GNSS/INS integrated unit is stated in (4), as shown at the bottom of the page, [10]; we specify the following quantities:

- $\mathbf{I}_{3\times3}$ is the identity matrix;
- $\mathbf{0}_{3\times3}$ is the zero matrix;
- $\boldsymbol{\Omega}^e_{ie,3\times3}$ is the skew-symmetric form of ω^e_{ie}, the Earth rotation rate expressed in ECEF frame;
- $\mathbf{R}^e_{b,3\times3}$ is the Direction Cosine Matrix (DCM) from body frame b to ECEF frame e;
- $diag(\boldsymbol{\alpha}_{1\times3})$ is a diagonal matrix for modelling the accelerometers bias states as first-order Gauss-Markov processes;
- $diag(\boldsymbol{\beta}_{1\times3})$ is a diagonal matrix for modelling the gyroscopes bias states as first-order Gauss-Markov processes;
- $\boldsymbol{w}_{f,3\times1}$ is the noise component affecting triaxial accelerometers as defined in (3);
- $\boldsymbol{w}_{\omega,3\times1}$ is the noise component affecting triaxial gyroscopes as defined in (3);
- $\boldsymbol{w}_{b_a,3\times1}$ is the driving noise for accelerometer bias drift [10];
- $\boldsymbol{w}_{b_g,3\times1}$ is the driving noise for gyroscope bias drift [10];
- $w_{\delta t_u}$ is the receiver clock bias noise;
- $w_{\delta \dot{t}_u}$ is the receiver clock drift noise;

As highlighted in (4) through curly under bracing, the dynamics matrix [10] $\mathbf{F}_{17\times17}$ defines the filtering system model and characterises the time evolution of navigation error states. The shaping matrix [10] $\mathbf{G}_{17\times14}$, instead, relates noise components on both sensor bias drift and receiver clock error to the states. Eventually, assuming time invariance of both matrices for the time interval over which the state estimation takes place, the state-transition matrix $\boldsymbol{\phi}_{k|k-1}$ and the process noise matrix $\boldsymbol{Q}_k$ of a discrete Kalman Filter (KF) can be derived from the continuous-time GNSS/INS system error model [10].

C. GNSS/INS MEASUREMENT MODEL

The observation model constitutes the layer that allows the integration filter to process raw GNSS measurements (i.e., pseudorange and Doppler-shift) and exploit them to construct a refined update to the error state estimate. In a tight

$$\begin{bmatrix} \dot{\boldsymbol{\delta r}}^e_{3\times1} \\ \dot{\boldsymbol{\delta v}}^e_{3\times1} \\ \dot{\boldsymbol{\epsilon}}^e_{3\times1} \end{bmatrix} = \begin{bmatrix} \boldsymbol{\delta v}^e_{3\times1} \\ -\mathbf{F}^e_{3\times3}\boldsymbol{\epsilon}^e_{3\times1} + \mathbf{N}^e_{3\times3}\boldsymbol{\delta r}^e_{3\times1} - 2\boldsymbol{\Omega}^e_{ie,3\times3}\boldsymbol{\delta v}^e_{3\times1} \\ -\boldsymbol{\Omega}^e_{ie,3\times3}\boldsymbol{\epsilon}^e_{3\times1} \end{bmatrix} + \begin{bmatrix} 0 \\ \mathbf{R}^e_{b,3\times3}\boldsymbol{\delta f}^b_{3\times1} \\ \mathbf{R}^e_{b,3\times3}\boldsymbol{\delta \omega}^b_{ib,3\times1} \end{bmatrix} \tag{2}$$

$$\begin{bmatrix} \dot{\boldsymbol{\delta r}}^e_{3\times1} \\ \dot{\boldsymbol{\delta v}}^e_{3\times1} \\ \dot{\boldsymbol{\epsilon}}^e_{3\times1} \\ \dot{\boldsymbol{\delta b}}^b_{a,3\times1} \\ \dot{\boldsymbol{\delta b}}^b_{g,3\times1} \\ \delta \dot{t}_u \\ \delta \ddot{t}_u \end{bmatrix} = \underbrace{\begin{bmatrix} \mathbf{0}_{3\times3} & \mathbf{I}_{3\times3} & \mathbf{0}_{3\times3} & \mathbf{0}_{3\times3} & \mathbf{0}_{3\times3} & \mathbf{0}_{3\times1} & \mathbf{0}_{3\times1} \\ \mathbf{N}^e_{3\times3} & -2\boldsymbol{\Omega}^e_{ie,3\times3} & -\mathbf{F}^e_{3\times3} & \mathbf{R}^e_{b,3\times3} & \mathbf{0}_{3\times3} & \mathbf{0}_{3\times1} & \mathbf{0}_{3\times1} \\ \mathbf{0}_{3\times3} & \mathbf{0}_{3\times3} & -\boldsymbol{\Omega}^e_{ie,3\times3} & \mathbf{0}_{3\times3} & \mathbf{R}^e_{b,3\times3} & \mathbf{0}_{3\times1} & \mathbf{0}_{3\times1} \\ \mathbf{0}_{3\times3} & \mathbf{0}_{3\times3} & \mathbf{0}_{3\times3} & -diag(\boldsymbol{\alpha}_{1\times3}) & \mathbf{0}_{3\times3} & \mathbf{0}_{3\times1} & \mathbf{0}_{3\times1} \\ \mathbf{0}_{3\times3} & \mathbf{0}_{3\times3} & \mathbf{0}_{3\times3} & \mathbf{0}_{3\times3} & -diag(\boldsymbol{\beta}_{1\times3}) & \mathbf{0}_{3\times1} & \mathbf{0}_{3\times1} \\ \mathbf{0}_{1\times3} & \mathbf{0}_{1\times3} & \mathbf{0}_{1\times3} & \mathbf{0}_{1\times3} & \mathbf{0}_{1\times3} & 0 & 1 \\ \mathbf{0}_{1\times3} & \mathbf{0}_{1\times3} & \mathbf{0}_{1\times3} & \mathbf{0}_{1\times3} & \mathbf{0}_{1\times3} & 0 & 0 \end{bmatrix}}_{\mathbf{F}_{17\times17}} \underbrace{\begin{bmatrix} \boldsymbol{\delta r}^e_{3\times1} \\ \boldsymbol{\delta v}^e_{3\times1} \\ \boldsymbol{\epsilon}^e_{3\times1} \\ \boldsymbol{\delta b}^b_{a,3\times1} \\ \boldsymbol{\delta b}^b_{g,3\times1} \\ \delta t_u \\ \delta \dot{t}_u \end{bmatrix}}_{\boldsymbol{\delta x}^e_{17\times1}} + \underbrace{\begin{bmatrix} \mathbf{0}_{3\times3} & \mathbf{0}_{3\times3} & \mathbf{0}_{3\times3} & \mathbf{0}_{3\times3} & \mathbf{0}_{3\times1} & \mathbf{0}_{3\times1} \\ \mathbf{R}^e_{b,3\times3} & \mathbf{0}_{3\times3} & \mathbf{0}_{3\times3} & \mathbf{0}_{3\times3} & \mathbf{0}_{3\times1} & \mathbf{0}_{3\times1} \\ \mathbf{0}_{3\times3} & \mathbf{R}^e_{b,3\times3} & \mathbf{0}_{3\times3} & \mathbf{0}_{3\times3} & \mathbf{0}_{3\times1} & \mathbf{0}_{3\times1} \\ \mathbf{0}_{3\times3} & \mathbf{0}_{3\times3} & \mathbf{I}_{3\times3} & \mathbf{0}_{3\times3} & \mathbf{0}_{3\times1} & \mathbf{0}_{3\times1} \\ \mathbf{0}_{3\times3} & \mathbf{0}_{3\times3} & \mathbf{0}_{3\times3} & \mathbf{I}_{3\times3} & \mathbf{0}_{3\times1} & \mathbf{0}_{3\times1} \\ \mathbf{0}_{1\times3} & \mathbf{0}_{1\times3} & \mathbf{0}_{1\times3} & \mathbf{0}_{1\times3} & 1 & 0 \\ \mathbf{0}_{1\times3} & \mathbf{0}_{1\times3} & \mathbf{0}_{1\times3} & \mathbf{0}_{1\times3} & 0 & 1 \end{bmatrix}}_{\mathbf{G}_{17\times14}} \underbrace{\begin{bmatrix} \boldsymbol{w}_{f,3\times1} \\ \boldsymbol{w}_{\omega,3\times1} \\ \boldsymbol{w}_{b_a,3\times1} \\ \boldsymbol{w}_{b_g,3\times1} \\ w_{\delta t_u} \\ w_{\delta \dot{t}_u} \end{bmatrix}}_{\mathbf{W}_{14\times1}} \tag{4}$$

architecture with indirect configuration, the integration filter uses, as input observation vector, the measurement misclosures [11]. Assuming N_s tracked satellites at epoch k, the *measurement misclosure* $\mathbf{z}_k$ is defined as:

$$\mathbf{z}_k = \boldsymbol{\zeta}_{GNSS,k} - \hat{\boldsymbol{\zeta}}_{INS,k} \tag{5}$$

where

- $\boldsymbol{\zeta}_{GNSS,k} = \left[\boldsymbol{\rho}_{GNSS,k},\ \dot{\boldsymbol{\rho}}_{GNSS,k}\right]^T$ is a column vector of size $2N_s \times 1$ collecting the raw GNSS pseudorange ($\boldsymbol{\rho}_k$) and pseudorange-rate measurements ($\dot{\boldsymbol{\rho}}_k$) from N_s satellites at k-th epoch;
- $\hat{\boldsymbol{\zeta}}_{INS,k} = \left[\hat{\boldsymbol{\rho}}_{INS,k},\ \hat{\dot{\boldsymbol{\rho}}}_{INS,k}\right]^T$ is a column vector of size $2N_s \times 1$ collecting the INS-based pseudorange and pseudorange-rate predictions related to the same set of N_s satellites;

Given the intrinsic non-linearity of GNSS-based multilateration, a first-order Taylor series approximation of pseudorange and pseudorange-rate equations can be used to retrieve a simplified, linear GNSS/INS observation model, as formulated in (6). A complete derivation and further details can be found in [4], [40], as shown at the bottom of the page. In particular, the geometry matrix [40] $\mathbf{H}_{\boldsymbol{\rho}}$ is computed as:

$$\mathbf{H}_{\boldsymbol{\rho}} = \begin{bmatrix} \frac{x_u - x_1}{R_1} & \frac{y_u - y_1}{R_1} & \frac{z_u - z_1}{R_1} \\ \frac{x_u - x_2}{R_2} & \frac{y_u - y_2}{R_2} & \frac{z_u - z_2}{R_2} \\ \vdots & \vdots & \vdots \\ \frac{x_u - x_{N_s}}{R_{N_s}} & \frac{y_u - y_{N_s}}{R_{N_s}} & \frac{z_u - z_{N_s}}{R_{N_s}} \end{bmatrix}_{N_s \times 3} \tag{7}$$

where $\mathbf{x}_u = \left(x_u, y_u, z_u\right)$ is the estimated receiver position in ECEF frame, $\mathbf{x}_j = \left(x_j, y_j, z_j\right)$ is the j-th satellite position in ECEF frame, and R_j is the Euclidean norm between the receiver location and the j-th satellite. Finally, $\mathbf{v}_k$ collects the residual errors affecting the measurement misclosures both in pseudorange and Doppler components. Assuming compensation of predictable error sources, $\mathbf{v}_k$ turns out to have zero-mean, jointly-Gaussian terms [1]:

$$\mathbf{v}_k = \mathcal{N}\left(\mathbf{0}, \mathbf{R}_k\right) \tag{8}$$

where the measurement noise covariance $\mathbf{R}_k$ is a diagonal matrix for uncorrelated satellite measurements.

D. UNSCENTED PARTICLE FILTER APPLIED TO GNSS/INS SCHEME

In the framework of Bayesian estimation over dynamic state space models, PFs still attract a remarkable research effort [17], [41]–[44]. They identify a family of simulation-based filtering techniques pursuing higher modelling flexibility over KFs. The hallmarks of a PF can be pinned up in the following two points [15], [45]:

- MC integration, which accomplishes a discrete, Dirac's Delta based approximation of posterior state densities through a finite set of simulated state samples;
- IS concept, which allows to randomly draw particles from a handy and known importance (or proposal) distribution that approximates the unknown posterior state density.

Relying on IS, a convenient choice of the proposal density is pivotal because it directly affects the particle generation process and, accordingly, it impacts on the occurrence rate of the unavoidable particles degeneracy phenomenon [16], [46]. Although heuristic techniques have been proposed to mitigate degeneracy and improving the importance accuracy [46], [47], a viable option is the Bayesian UPF architecture, which considers a linear regression of weighted state samples [48]. First defined in [21], it is a hybrid scheme consisting of a baseline PF which exploits, as a feeding stage, an UKF to frame out an accurate enough proposal fitting with the unknown a-posteriori distribution. A simple block diagram illustrating the main stages of the UPF routine is shown in Fig. 2. At every estimation epoch, the UKF posterior state mean and covariance estimates from measurement updates are exploited to define a new importance density that, correspondingly, drives the particles sampling. After computing their importance weights, the posterior state mean and covariance estimates are updated and further refined [21], [22], [28], [49]. For ease of comprehension, the interested reader can refer to [21] which collects few details and proposes a formalization for each building block reported in Fig. 2.

III. ENHANCED UPF ARCHITECTURE WITH ROBUSTNESS OPTIMISATION

Given the discussed framework in Section II for a UPF-based GNSS/INS tight unit, this Section presents the adaptive noise model optimization and the robustness countermeasures embedded in the high-complexity AUPF architecture

$$\begin{bmatrix} \boldsymbol{\rho}_{GNSS,k} - \hat{\boldsymbol{\rho}}_{INS,k} \\ \dot{\boldsymbol{\rho}}_{GNSS,k} - \hat{\dot{\boldsymbol{\rho}}}_{INS,k} \end{bmatrix}_{2N_s \times 1} = \underbrace{\begin{bmatrix} \mathbf{H}_{\boldsymbol{\rho},N_s \times 3} & \mathbf{0}_{N_s \times 3} & \mathbf{0}_{N_s \times 9} & \mathbf{1}_{N_s \times 1} & \mathbf{0}_{N_s \times 1} \\ \mathbf{0}_{N_s \times 3} & \mathbf{H}_{\boldsymbol{\rho},N_s \times 3} & \mathbf{0}_{N_s \times 9} & \mathbf{0}_{N_s \times 1} & \mathbf{1}_{N_s \times 1} \end{bmatrix}}_{\mathbf{H}_{k,2N_s \times 17}} \underbrace{\begin{bmatrix} \boldsymbol{\delta r}^e_{3\times 1} \\ \boldsymbol{\delta v}^e_{3\times 1} \\ \boldsymbol{\epsilon}^e_{3\times 1} \\ \boldsymbol{\delta b}^b_{a,3\times 1} \\ \boldsymbol{\delta b}^b_{g,3\times 1} \\ \delta t_u \\ \dot{\delta t}_u \end{bmatrix}}_{\boldsymbol{\delta x}^e_{17\times 1}} + \mathbf{v}_k \tag{6}$$

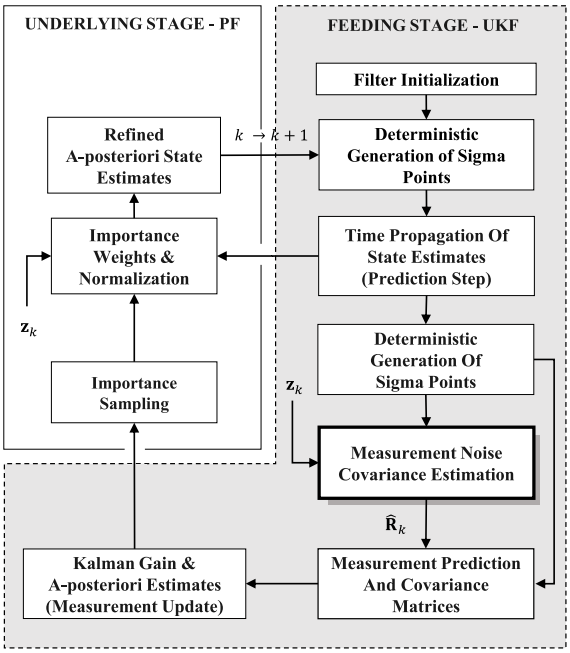

FIGURE 2. Simplified block diagram of the UPF algorithm composed by a UKF-based feeding stage and a PF-based underlying stage. The input GNSS measurement misclosure $\mathbf{z}_k$ and the noise covariance matrix $\mathbf{R}_k$ are highlighted.

proposed by this paper. Specifically, the measurement noise covariance estimation block of Fig. 2 is enhanced through the adaptive structure depicted in Fig. 3, which implements a mitigation of misleading biases affecting input GNSS misclosures retrieved in compromised signal environments.

A. ADAPTIVE COVARIANCE ESTIMATION BASED ON REDUNDANT MEASUREMENTS

Focusing on measurement noise covariance ($\mathbf{R}_k$) models, baseline UPF architectures rely on parameter estimation, which leverages functional relations to compute the variance of each misclosure. For example, both satellite elevation and received carrier-to-noise-density ratio (C/N_0) are common indexes to weight the components of the observation vector $\mathbf{z}_k$ [26].

Although real-time tunable, the use of parameters limits to few degrees of freedom the stochastic noise characterisation resulting into a nearly static (i.e., semi-static) estimation. For GNSS/INS integrated units with high-grade Micro Electro-Mechanical System (MEMS) IMUs, the stochastic part of inertial measurement errors can be considered constant, but the same may not apply for GNSS measurements [50]. This usually happens in signal degraded environments with highly changing dynamics, like urban canyons, and this heavily affects both filter accuracy and robustness.

Adaptive noise modelling strategies, instead, weakly rely on a-priori statistical information and aim at enhancing the estimation performance by exploiting the filter learning process based on the sequence of input innovations [27]. As such, any change in the external environment directly reflects on noise and on its stochastic properties which dynamically

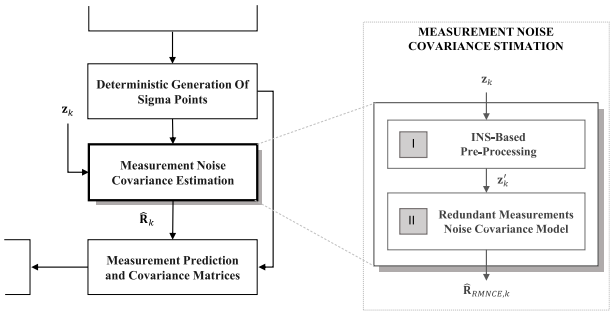

FIGURE 3. Insight on the measurement noise covariance estimation block of Fig. 2 for the enhanced RMNCE-based AUPF architecture with embedded robustness countermeasures. The GNSS measurement misclosure $\mathbf{z}_k$ feeds the input of block I, where the GNSS-based pseudorange misclosures are filtered to mitigate misleading bias injections.

update the filter statistical information and tune the error parametrization characterising input observables.

In this paper, an AUPF architecture is considered that exploits RMNCE strategy (Fig. 3, block II). This method adapts observation noise statistics by relying on redundant information retrieved from two independent measurement systems [51]. The main advantage of the RMNCE approach is in that noise modelling is strictly based on measurements and is fully independent from the system states and their related estimation errors.

The RMNCE underlying principle assumes the existence of two independent redundant measurements for the same quantity, and computes the variance of such quantity by suitably processing the difference between the two measurements [52]. Specifically, let's consider $Z_1(k)$ and $Z_2(k)$ two independent redundant measurements, coming from two different sources, of the same quantity Z_k. They can be expressed as follows [52]:

$$Z_i(k) = Z(k) + S_i(k) + V_i(k) \quad i = \{1, 2\} \tag{9}$$

where $S_i(k)$ identifies unknown system noise, while $V_i(k)$ corresponds to uncorrelated, zero-mean measurement noise. For both measurement systems, it is possible to define First-Order Self-Differences (FOSDs) $\Delta Z_i(k)$ according to [51]:

$$\Delta Z_i(k) = Z_i(k) - Z_i(k-1) \quad i = \{1, 2\} \tag{10}$$

and, assuming that $S_i(k) - S_i(k-1) \simeq 0$, it is possible to write:

$$\Delta Z_i(k) = [Z(k) - Z(k-1)] + [V_i(k) - V_i(k-1)]$$

From (10), it can be understood that FOSDs compute a discrete approximation of the first-order derivative of each redundant measurement with respect to epoch time k. Hence, $\Delta Z_1(k)$ and $\Delta Z_2(k)$ carry information about the variation of each observable over consecutive epochs.

Moreover, a Second-Order Mutual Difference (SOMD) $\Delta Z_{1,2}(k)$ can be specified [51]:

$$\Delta Z_{1,2}(k) = \Delta Z_1(k) - \Delta Z_2(k) \tag{11}$$

which depends solely on noises affecting redundant measurements and expresses the residual between their derivatives. Based on the proposed equations, the variances of $Z_1(k)$ and $Z_2(k)$ can be simultaneously retrieved according to (12), as shown at the bottom of the page, where $\mathbb{E}\left(\Delta Z_{1,2}(k)\,\Delta Z_{1,2}^T(k)\right)$, $\mathbb{E}\left(\Delta Z_1(k)\,\Delta Z_1^T(k)\right)$ and $\mathbb{E}\left(\Delta Z_2(k)\,\Delta Z_2^T(k)\right)$ are the discrete auto-correlations of $\Delta Z_{1,2}(k)$, $\Delta Z_1(k)$ and $\Delta Z_2(k)$, respectively.

In the integrated unit under analysis, GNSS and INS act as the two independent measurement systems to meet the RMNCE hypothesis; on one hand, the GNSS receiver directly supplies noisy pseudorange and Doppler-shift observables to the fusion algorithm while, on the other hand, the inertial body position and velocity estimates from the INS can be used to predict the same GNSS-based data.

Accounting for the unpredictability and variability of the external environment along the trajectory, few refinements can still be pursued on the RMNCE method. First, the estimation of the auto-correlations in (12) can be averaged over a sliding window thereby tracking real-time noises more accurately and mitigating the effects of historical information [52]. Second, it is useful to monitor the stability of each tracked satellite inside the window; as a matter of fact, a highly fluctuating satellite which is occasionally tracked should not contribute to the noise characterisation since it would likely cause overestimation of the measurement variance.

B. ADAPTIVE PRE-PROCESSING ON INPUT MEASUREMENTS

The RMNCE method, recalled in Section III-A, despite enabling a flexible tuning of misclosures statistics, is definitely not enough to hit the desired robustness of the state estimation. In fact, by relying on measurements only, spurious variance glitches of biased misclosures can anyway jeopardise the covariance tuning and spoil the state estimation as well. Moreover, multipath changes very fast in urban and induces both positive and negative biases; hence, the historical information included within the sliding window may not correctly describe multipath-related error statistics.

Given these premises, adaptive covariance estimation is complemented with a novel signal processing stage - block I in Fig. 3 - aimed at enhancing both adaptivity and robustness of the discussed tight GNSS/INS scheme. For sake of clarity, it is to remark that such an original contribution does not replace the aforementioned adaptive covariance estimation module, but just prepends to it in order to filter out unpredictable biases corrupting the GNSS-based measurement misclosures (5). In details, it foresees a self-contained, low-complexity pre-processing algorithm operating a real-time dynamic smoothing of input misclosures to automatically mitigate undesired bias injections in presence of multipath. Then, error covariance matrix calculation leverages pre-processed measurements, thus taking advantage of its action. It is important to highlight that, within this paper, pre-processing is applied to pseudorange misclosures only, thus leaving for future investigation a convenient tailoring to Doppler-shift misclosures (i.e. pseudorange rates) as well.

The pre-processing module builds on a two-stage architecture including a initialisation block, needed to define and configure parameters useful to the algorithm, and an operational block, which implements the core routine to smooth out misleading bias injections.

At a generic epoch k, the GNSS receiver is supposed to track M satellites, and two main quantities can be tuned:

- σ_k, the estimated standard deviation of ranging misclosures in open-sky conditions (that is, in absence of unmodelled multipath effects).
- N pre-processing quantization levels based on σ_k, such that to guarantee a sufficient adaptivity.

Then, few assumptions must hold in order to feed the pseudocode reported in Algorithm 1:

- Knowledge of GNSS code-based pseudorange measurements of visible satellites $\{\rho^i_{GNSS,k}\}_{i=1}^M$;
- Knowledge of nominal user-to-satellite ranges $\{\hat{\rho}^i_{INS,k}\}_{i=1}^M$ retrieved from INS-based predictions at epoch k;
- Knowledge of the cumulative means of pseudorange misclosures $\{\mu^i_{\boldsymbol{\rho},k-1}\}_{i=1}^M$ computed at previous epoch $k-1$;

Based on these quantities, the proposed approach implements a real-time, multi-level magnitude scaling (i.e., quantization) of the pseudorange component characterising the input misclosure vector $\mathbf{z}_k$ (5)

$$\mathbf{z}_{\boldsymbol{\rho},k} = \boldsymbol{\rho}_{GNSS,k} - \hat{\boldsymbol{\rho}}_{INS,k} \tag{13}$$

by contemplating possible bias trends which are tracked through the cumulative average $\mu_{\boldsymbol{\rho},k-1}$, kept updated up to epoch $k-1$.
In particular, for each satellite i, the magnitude of the residual pseudorange misclosure

$$f\left(\mathbf{z}^i_{\boldsymbol{\rho},k}, \mu^i_{\boldsymbol{\rho},k-1}\right) = |\mathbf{z}^i_{\boldsymbol{\rho},k} - \mu^i_{\boldsymbol{\rho},k-1}|. \tag{14}$$

$$\begin{aligned}
\sigma_1^2 &= \frac{\mathbb{E}\left(\Delta Z_{1,2}(k)\,\Delta Z_{1,2}^T(k)\right) + \mathbb{E}\left(\Delta Z_1(k)\,\Delta Z_1^T(k)\right) - \mathbb{E}\left(\Delta Z_2(k)\,\Delta Z_2^T(k)\right)}{4} \\
\sigma_2^2 &= \frac{\mathbb{E}\left(\Delta Z_{1,2}(k)\,\Delta Z_{1,2}^T(k)\right) - \mathbb{E}\left(\Delta Z_1(k)\,\Delta Z_1^T(k)\right) + \mathbb{E}\left(\Delta Z_2(k)\,\Delta Z_2^T(k)\right)}{4}
\end{aligned} \tag{12}$$

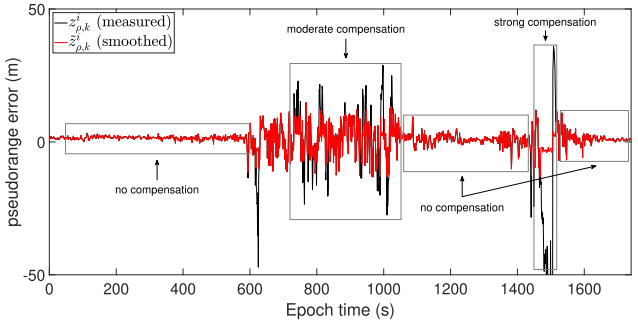

FIGURE 4. Effect of the pre-processing module on a real GNSS/INS pseudorange misclosure retrieved from L1/CA signal of GPS PRN32.

is compared against an adaptive threshold

$$g(\sigma_k, p) = 2^p \cdot \sigma_k \quad p \in (1, N) \tag{15}$$

to identify the correct pre-processing quantization level. Whenever the condition

$$f\left(\mathbf{z}^i_{\boldsymbol{\rho},k}, \mu^i_{\boldsymbol{\rho},k-1}\right) \leq g(\sigma_k, p)$$

gets satisfied, the pseudorange error sample $\mathbf{z}^i_{\boldsymbol{\rho},k}$ is synthetically reduced to

$$\tilde{\mathbf{z}}^i_{\boldsymbol{\rho},k} = \frac{\mathbf{z}^i_{\boldsymbol{\rho},k}}{2^{p-1}} \tag{16}$$

Algorithm 1 Pseudorange Pre-Processing (Error-Based Formulation) for Tight GNSS/INS Integrated Navigation System, at Given Epoch k

1: **for** $i = 1$ to M **do**
2: **for** $p = 1$ to N **do**
3: Compute $f\left(\mathbf{z}^i_{\boldsymbol{\rho},k}, \mu^i_{\boldsymbol{\rho},k-1}\right)$ (14) and $g(\sigma_k, p)$ (15)
4: **if** $f\left(\mathbf{z}^i_{\boldsymbol{\rho},k}, \mu^i_{\boldsymbol{\rho},k-1}\right) \leq g(\sigma_k, p)$ **then**
5: $$\tilde{\mathbf{z}}^i_{\boldsymbol{\rho},k} = \frac{\mathbf{z}^i_{\boldsymbol{\rho},k}}{2^{p-1}}$$
6: **end if**
7: **end for**
8: **end for**
9: Update cumulative mean for the i-th satellite at epoch k:
$$\mu^i_{\boldsymbol{\rho},k} = \mu^i_{\boldsymbol{\rho},k-1} + \frac{\tilde{\mathbf{z}}^i_{\boldsymbol{\rho},k}}{k}$$

This adaptive pre-processing is generally capable to preserve the possible error trends hidden by multipath-induced fluctuations; the adoption of an adaptive scaling of the misclosures over multiple quantization levels guarantees the abortion of error outliers without affecting the low-frequency, zero-mean noise like pattern which is due to a blending of inertial bias drift, inertial data noise and possible, residual contributions.

The envisioned methodology bears multiple advantages. First of all, it reduces the pseudorange misclosure $\mathbf{z}^i_{\boldsymbol{\rho},k}$ as soon as it is measured, without introducing any latency or requiring any extra buffering to keep memory of measured misclosures in previous epochs. Secondly, the amount of extra complexity added to the filtering algorithm is rather negligible. Furthermore, the proposed strategy is independent from the investigated scenarios. Hence, it is expected to be effective to compensate for a variety of undesired bias effects. Last, but not least, acting as a standalone module, it is fully portable and does not inhibit the normal flow of the Bayesian integration routine.

An example of the pre-processing outcome is provided in Fig. 4, where the proposed methodology is applied to GNSS/INS pseudorange misclosure obtained from L1/CA signal of Global Positioning System (GPS) Pseudo Random Noise (PRN) 32. The adaptivity of the pre-processing algorithm guarantees

- unaltered misclosure trend in nominal open-sky conditions (i.e., no compensation);
- moderate misclosure reduction in presence of fast, remarkable bias fluctuations;
- heavy error compensation against intense fluctuations.

IV. PERFORMANCE ASSESSMENT IN URBAN SETTING

The scope of the forthcoming assessment is to verify the accuracy performance of the high-complexity Bayesian AUPF architecture embedding the robustness optimizations defined throughout Section III, when compared against both i) plain UPF architecture (Section II-D) and ii) the most popular AUPF formulation based on RAE algorithm for measurement noise covariance estimation.

A. EXPERIMENTAL SETUP & METHODOLOGY

To validate the proposed solution, a dataset was selected among the ones available in our repository because of its relevant features in terms of multipath and environmental characteristics. The dataset was collected on a car ride in a urban area nearby Politecnico di Torino (Turin, Italy) in November 4, 2015 at 12:16 UTC, with a total duration of 39 minutes. The vehicle was driven along a path characterised by narrow streets surrounded by buildings and trees, limiting satellites visibility and inducing GNSS signal degradation. For the experiment, an embedded board was mounted on the vehicle supplying both GNSS ranging data and inertial data in real-time. In details, the following commercial modules composed the hardware testbench:

- a low-cost, mass-market GPS receiver (i.e. the NVS NV08C-CSM). Such positioning module is commonly used in consumer-grade devices for road navigation. It supplies low-rate noisy pseudorange and Doppler-shift measurements;
- a consumer-grade MEMS-technology strapdown IMU (i.e. TDK InvenSense MPU-9250), including two triads of accelerometers and gyroscopes. It supplies high-rate specific force and angular rate measurements.

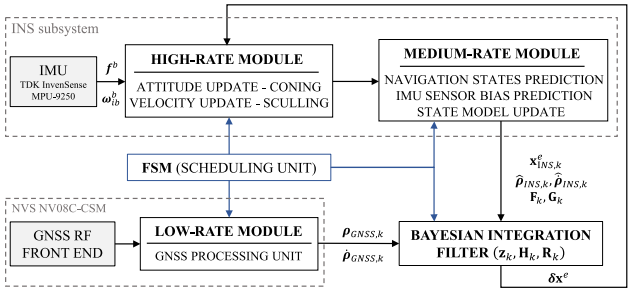

FIGURE 5. Block diagram of the integration software for the real-time simulation of a GNSS/INS tight architecture. Scheduling commands from the FSM unit are included in the diagram with cyan arrows.

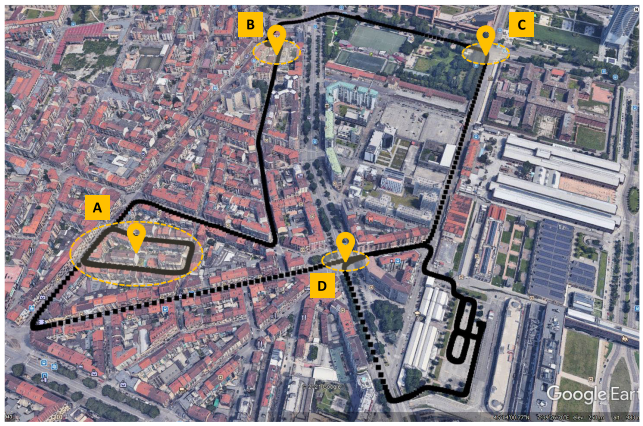

FIGURE 6. Map view of the ground reference for the tested vehicular trajectory in the final assessment dataset (Note: images are taken via Google Earth Pro software by Google LLC.).

In parallel to the foregoing modules, benchmark measurements were retrieved by means of a dual-frequency, survey-grade GNSS receiver, combined with a tactical-grade IMU (i.e., Novatel SPAN-CPT). Such a reference receiver provides real-time localization at sub-decimetre level accuracy and is commonly employed for applications in the professional segment. As such, this positioning sensor has been included in the experimental setup to grant a highly accurate ground truth (i.e., reference trajectory) useful for the estimation of errors in the navigation solution from the tightly-integrated unit. For the assessment of the considered Bayesian integration routines, a MATLAB®-based, fully-software emulator of a GNSS/INS tightly integrated navigation system has been run in post-processing on the collected dataset. For sake of rigorousness, simulations are run on a subset of the whole dataset which includes relevant epochs for the vehicle dynamics. As such, with an integration rate of 1 Hz, 1740 epochs (29 minutes) will be hence shown in the results of Section V.

Within the emulation environment, a FSM manages the scheduling of input observables and assigns timestamps separately to both inertial data and raw GNSS measurements to grant synchronization between the two positioning sensors. In details, the GNSS rate is set to 1 Hz (it eventually constrains the integration rate), while the INS rate is fixed to 10 Hz with an IMU rate of 100 Hz. A simplified

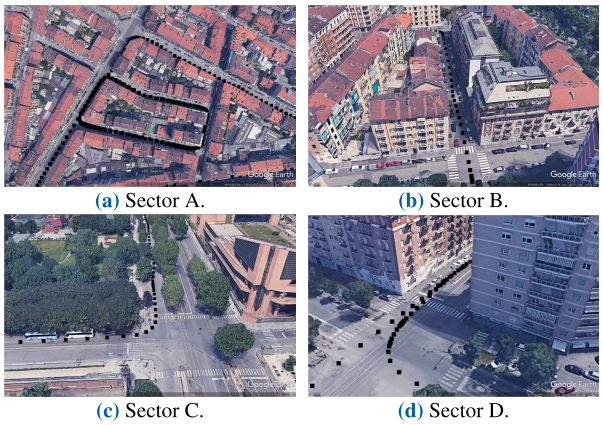

(a) Sector A. (b) Sector B. (c) Sector C. (d) Sector D.

FIGURE 7. Challenging navigation environments encountered along the experimental trajectory in the analysed urban dataset. Each black dot represents 1 Hz positioning solutions of the Novatel SPAN-CPT (Note: images are taken via Google Earth Pro software by Google LLC.).

schematic representation of the integration software is provided in Fig. 5.

Every 0.010 s, a new set of IMU measurements is produced and coning and sculling integrals are solved [53], [54]. Due to non linearities of inertial motion, it is fundamental to compute these integrals at high rate (high-rate module in Fig. 5). In this way, the change of orientation and velocity are tracked with high temporal granularity and the medium-rate predictions to the absolute position, velocity and attitude states can be dead-reckoned at the lower rate of 10 Hz, that is every 0.100 s (medium-rate module in Fig. 5). Clearly, all these operations are executed within the INS subsystem. Whenever a new set of GNSS noisy observables becomes available (low-rate module in Fig. 5), the integration filter produces an estimate of the error state vector (1) by relying on process (4) and measurement (6) models.

Based on this setting and targeting the horizontal state estimation accuracy as primary performance indicator, the spatial components related to the vehicle horizontal position are object of investigation. In this sense, the vertical position (i.e., body geodetic height) is not examined since it is typically penalised by the geometry of the GNSS-based multilaterion problem. Then, the Root-Mean-Square Error (RMSE) metric is adopted to quantify the accuracy of the tightly integrated navigation solution.

The ground-truth path for the tested urban trajectory is shown in Fig. 6. In the forthcoming results, special attention is devoted to few trajectory sectors characterised by heterogeneous features:

- Sectors A and B identify deep urban settings with limited visibility of satellites, poor geometry and potentially strong multipath and shadowing effects.
- Sector C corresponds to a mild urban context with dense foliage but better visibility conditions than sectors A and B.
- Sector D, a crossroad that determines a cut-off slice of the vehicle path where the average accuracy performance of any Bayesian hybridisation routine tends to

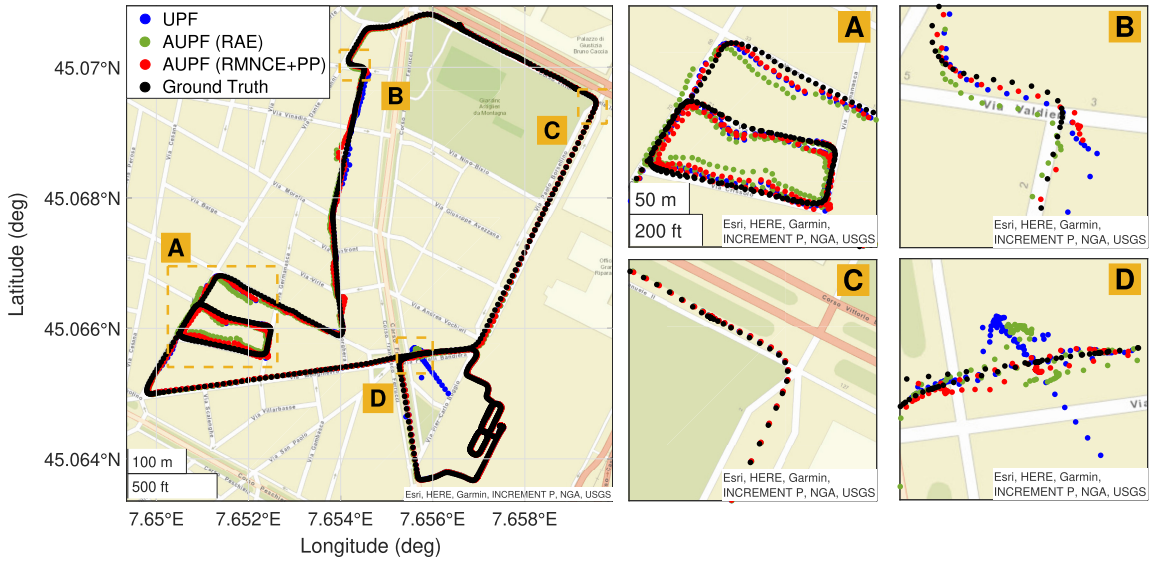

FIGURE 8. 2D experimental trajectories in latitude/longitude (LLH) spherical coordinates. Comparison between UPF, RAE-based AUPF, RMNCE-based AUPF with Pre-Processing (PP) and ground truth. Each dot represents an integration epoch.

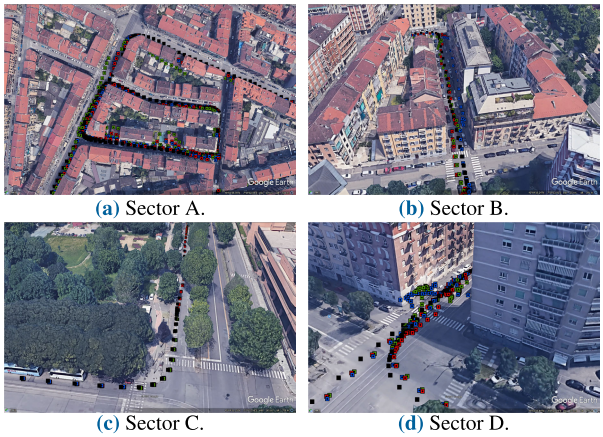

(a) Sector A. (b) Sector B.

(c) Sector C. (d) Sector D.

FIGURE 9. Highlight of the experimental trajectories in the challenging sectors along the experimental trajectory involved in the analyzed urban dataset. Comparison between UPF (blue), RAE-based AUPF (light green), RMNCE-based AUPF with Pre-Processing (red) and ground reference (black). (Note: images are taken via Google Earth Pro software by Google LLC.)

dramatically worsen, likely due to the presence of highly reflective and diffractive surfaces.

To have a deeper understanding of these challenging scenarios, Fig. 7 captures a snapshot for each indicated sector.

B. FILTERS CONFIGURATION

The proposed analysis leverages PF-based hybrid architectures employing a fixed number of 1000 particles for the estimation update of navigation states, including position, velocity and time (i.e., clock bias and drift components) unknowns. The remaining bias states, associated to IMU sensors measurements, are just propagated from the feeding UKF stage, thus leveraging a marginalised estimation [55]. No rules of thumb have been defined to select an adequate number of particles to be used. Typically, this aspect is managed either with an oversized value, involving a waste of computational resources, or by addressing adaptive solutions that are out of the scope of this study [56]. Such a configuration holds for all the three architectures investigated throughout the following analysis.

V. RESULTS

The analysis of the pursued experimental outcomes from the assessment is organized as follows. Section V-A provides an overview of the horizontal position estimates in qualitative terms by looking at simulated vehicle trajectories. Then, Section V-B supplies a detailed accuracy performance analysis about horizontal error statistics characterising the same trajectories.

A. QUALITATIVE ANALYSIS ON EXPERIMENTAL PATHS

Fig. 8 compares the experimental vehicle trajectory, estimated by both plain and adaptive UPF architectures, with respect to the sub-decimetre accurate ground reference. As an additional visual aid, the same figure integrates the zooms on the challenging sectors (refer to Section IV-A) highlighted throughout the assessment, which have been found to critically undermine both the robustness of the filter estimation and the integrity of the navigation solution. These sectors are also captured in the Google Earth snapshots of Fig. 9. Starting from the mild urban setting characterising sector C, the positioning solutions supplied by the different PF-based stages are largely matching each other; this can be better caught in Fig. 9c. Moving to more critical trajectory slices immersed in deep urban context (sector A in Fig. 9a and sector B in Fig. 9b), multipath-related biasing effects in the estimated vehicle positions are standing out. In particular, looking at sector A and accounting for AUPF stages only, the proposed RMNCE-based scheme appears more robust against unmodelled error sources and pursues higher accuracy over the

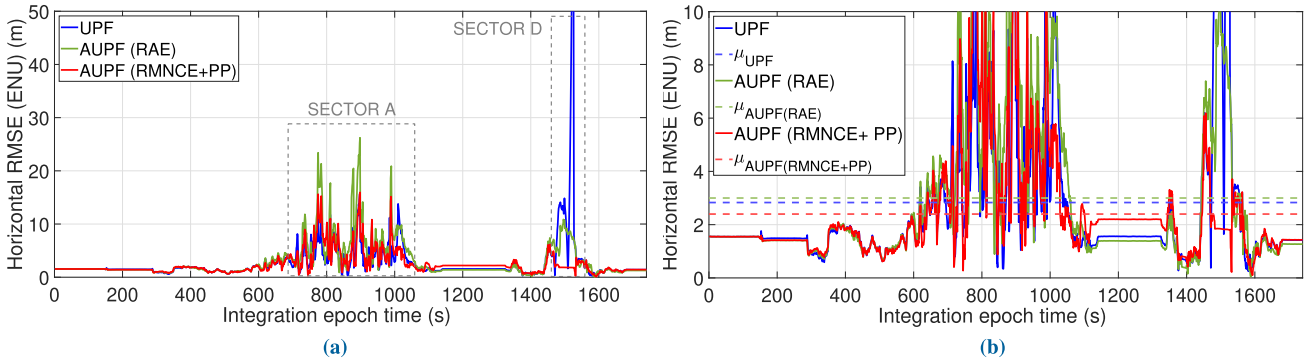

FIGURE 10. (a) RMSE on the horizontal position (Easting/Northing) in UTM-coordinates. For readability reasons, the indications of Sectors B and C are omitted. (b) Highlight of the mean horizontal RMSE over the experimental dataset. Comparison between plain UPF, RAE-based AUPF and the proposed RMNCE-based AUPF with Pre-Processing (PP). A fixed number of 1000 particles is considered.

RAE-based solution. Such a result stems from a blend of two effects

- the INS-based pre-processing stage which conditions GNSS ranging measurements to absorb misleading multipath-related biases.
- the measurement covariance computation by the RMNCE strategy which further attenuates the impact of unmodelled bias sources;

Interestingly, in such scenarios, a semi-static UPF formulation (i.e., plain architecture) still grants comparable horizontal accuracy performance with reference to adaptive solutions.

Instead, moving to sector D (Fig. 8 and Fig. 9d), which identifies an area surrounded by highly reflective buildings with critically enhanced multipath scattering, adaptive filters are unequivocally outperforming the plain UPF stage, whose estimated position fixes are quickly diverging. Narrowing the sight on AUPF schemes, the considered RMNCE-based AUPF with pre-processing preserves a higher accuracy level in the horizontal position estimates over the RAE-based variant, and it delivers a smoother trajectory estimate without experiencing any error bouncing phenomenon.

B. AUPF ERROR STATISTICS WITH ENHANCEMENT TECHNIQUES

First, the analysis of the horizontal RMSE as a function of the integration epochs for the tested urban data set (Section IV) is proposed in Fig. 10a, where the enhanced AUPF architecture with pre-processing is compared against both a plain UPF scheme (Section II-D) and a RAE-based AUPF stage (Section III-A). In particular, the critical trajectory sectors A (Fig. 7a) and D (Fig. 7d) are highlighted, where the average horizontal error increments (i.e., mean error jumps) are rather blatant. Such biasing effects are caused by the presence of tall buildings - and possibly other environmental obstacles - obstructing Line-of-sight (LOS) propagation and enhancing scattering phenomena (i.e., multipath). Moreover, observing the global RMSE trend, it can be evidenced the presence of a steady bias floor amounting to about 1.5 m, which is caused by some alignment problems in the tactical-grade IMU within the survey-grade GNSS receiver employed to retrieve a ground truth. Although the RMSE lines for the different PF-based architectures extensively match each other when travelling mild areas in near open-sky conditions, the high-complexity RMNCE-based AUPF stage with pre-processing grants superior robustness under signal degraded scenarios and prevents the error from drifting unbounded. This effect is moderately observable in Sector A - where plain UPF is robust as well - but gets definitely marked in the final part of the dataset. In fact, especially in Sector D, the proposed Bayesian solution manages to bound the maximum error below 3 m, while the RAE-based stage allows a higher error bias increase and the plain architecture is even diverging (i.e, the maximum RMSE touches 110 m). The improved robustness and accuracy performance of enhanced AUPF solution in harsh navigation conditions results from combining the dynamic pre-processing module (Section III) with RMNCE technique. As far as the latter is concerned, the computation of $\mathbf{R}_k$ involves FOSDs (10), which correspond to an approximated, discrete, first-order derivative. Therefore, considering a sufficiently wide buffer of collected pseudorange and Doppler measurements, the derivative over the buffer implements a basic low-pass filtering which can help in mitigating multipath-related bias injections.

To better catch the horizontal accuracy improvement achieved by the proposed architecture, Fig. 10b bounds the dynamic RMSE range to 10 m and highlights the mean horizontal error over the analyzed dataset for each Bayesian filter. As a matter of fact, the RMNCE-based AUPF with pre-processing gives the smallest mean error - highest average accuracy - of 2.4 m, which corresponds to an average accuracy improvement of 0.43 m (i.e., 15.19 %) over a plain UPF solution (which measures an average RMSE of 2.83 m) and of 0.6 m (i.e., 20 %) over a RAE-based AUPF variant (which measures an average RMSE of 3 m).

For further investigation, Fig. 11 illustrates the Empirical Cumulative Density Function (ECDF) curves of the RMSE on the horizontal position in Universal Transverse Mercator (UTM) coordinates, together with zooms at few percentiles

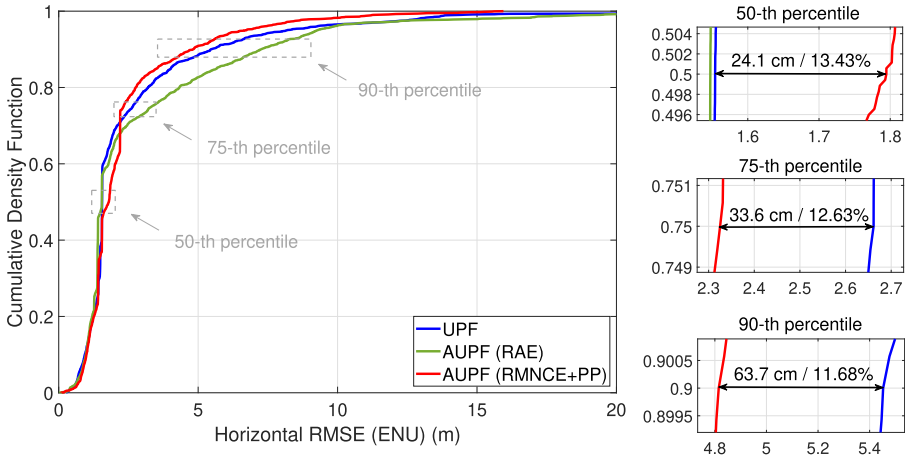

FIGURE 11. Empirical CDF (ECDF) of the RMSE on the horizontal position (Easting/Northing) in UTM-coordinates. Comparison between UPF, RAE-based AUPF and the proposed RMNCE-based AUPF with Pre-Processing (PP). A fixed number of 1000 particles is considered.

TABLE 1. Horizontal (E/N) position RMSE measured, for the analysed UPF and AUPF architectures, at 50-th, 75-th and 90-th percentiles. A fixed number of 1000 particles is considered.

UPF architecture	50-th perc. Error (m)	75-th perc. Error (m)	90-th perc. Error (m)
AUPF (RMNCE+Pre-Proc.)	1.795	2.325	4.815
AUPF (RAE)	1.547	3.325	7.258
Plain UPF	1.554	2.661	5.452

of interest. Starting from the high accuracy segment (horizontal RMSE within 2 m), there is no relevant accuracy performance difference among the considered filters up to the 40-th percentile. However, between the 40-th and 70-th levels, the enhanced AUPF architecture is losing few tens of centimetres over the other PF-based schemes. In particular, based on the measured RMSEs at the 50-th percentile specified in Table 1, the accuracy penalty amounts to 0.24 m (i.e., 13.43 %) over the UPF and to 0.25 m (i.e., 13.82 %) over the AUPF with RAE. Nevertheless, above the 70-th percentile, the Cumulative Density Function (CDF) trends overturn and the RMNCE-based AUPF compensates the foregoing performance loss. At the 75-th percentile, it achieves 30.08 % (i.e., 1 m) accuracy enhancement over the RAE-based AUPF and 12.63 % (i.e., 0.34 m) over a plain UPF (Table 1). Furthermore, at the 90-th percentile, the measured gains are 33.66 % (i.e., 2.44 m) over the RAE-based AUPF and 11.68 % (i.e., 0.64 m) over the UPF.

VI. CONCLUSION

Although several advanced estimation algorithms are exploited in positioning applications to tightly integrate GNSS and INS, their robustness against biased input measurements is still concerned. Hybrid estimators such as UPF can effectively host adaptive stages to counteract the detrimental effects of multipath in harsh environment. The proposed, enhanced AUPF architecture exploits an adaptive logic composed by a pre-processing stage and a run-time error covariance estimation, i.e. RMNCE, to improve navigation accuracy and estimation robustness over both a plain UPF and a RAE-based AUPF architectures. The experimental assessment on a urban, vehicular trajectory shows an improvement of the horizontal positioning error of more than 10 % above the 75-th percentile and demonstrates the superior adaptivity of the RMNCE method against RAE.

REFERENCES

[1] R. Conley, R. Cosentino, E. Kaplan, C. Hegarty, J. Leva, M. DeHaag, and K. Van Dyke, "Performance of stand-alone GPS," in *Understanding GPS: Principles and Applications*, 2nd ed. Norwood, MA, USA: Artech House, 2017, ch. 7, pp. 21–63. [Online]. Available: https://us.artechhouse.com/Understanding-GPSGNSS-Principles-and-Applications-Third-Edition-P1871.aspx

[2] P. Ward, J. Betz, and C. Hegarty, "Interference, multipath, and scintillation," in *Understanding GPS: Principles and Applications*, 2nd ed. Norwood, MA, USA: Artech House, 2017, ch. 6, pp. 21–63. [Online]. Available: https://us.artechhouse.com/Understanding-GPSGNSS-Principles-and-Applications-Third-Edition-P1871.aspx

[3] P. Xie and M. G. Petovello, "Measuring GNSS multipath distributions in urban canyon environments," *IEEE Trans. Instrum. Meas.*, vol. 64, no. 2, pp. 366–377, Feb. 2015.

[4] E. Kaplan, J. Leva, D. Milbert, and M. Pavloff, "Fundamentals of satellite navigation," in *Understanding GPS: Principles and Applications*, 2nd ed. Norwood, MA, USA: Artech House, 2017, ch. 2, pp. 21–63. [Online]. Available: https://us.artechhouse.com/Understanding-GPSGNSS-Principles-and-Applications-Third-Edition-P1871.aspx

[5] P. Aggarwal, N. El-Sheimy, A. Noureldin, and Z. Syed, *MEMS-Based Integration Navigation*. Norwood, MA, USA: Artech House, 2010.

[6] P. Groves, *Principles of GNSS, Inertial, and Multisensor Integrated Navigation Systems*, 2nd ed. London, U.K.: Artech House, 2013.

[7] A. Noureldin, T. Karamat, and J. Georgy, "INS/GPS integration," in *Fundamentals of Inertial Navigation, Satellite-Based Positioning and Their Integration*. Cham, Switzerland: Springer, 2013, ch. 8, pp. 247–271, doi: 10.1007/978-3-642-30466-8.

[8] A. Schutz, D. E. Sanchez-Morales, and T. Pany, "Precise positioning through a loosely-coupled sensor fusion of GNSS-RTK, INS and LiDAR for autonomous driving," in *Proc. IEEE/ION Position, Location Navigat. Symp. (PLANS)*, Apr. 2020, pp. 219–225.

[9] G. Falco, M. Pini, and G. Marucco, "Loose and tight GNSS/INS integrations: Comparison of performance assessed in real urban scenarios," *Sensors*, vol. 17, no. 2, p. 255, Jan. 2017, doi: 10.3390/s17020255.

[10] M. Petovello, "Real-time integration of a tactical-grade IMU and GPS for high-accuracy positioning and navigation," Ph.D. dissertation, Dept. Geomatics Eng., Univ. Calagary, Calgary, AB, Canada, Apr. 2003. [Online]. Available: http://www.geomatics.ucalgary.ca/links/GradTheses.html

[11] M. Petovello, C. O'Driscol, and G. Lachapelle, "Weak signal carrier tracking using extended coherent integration with an ultra-tight GNSS/IMU receiver," in *Proc. Eur. Navigat. Conf.*, 2008, pp. 23–25. [Online]. Available: https://schulich.ucalgary.ca/labs/position-location-and-navigation/node1354

[12] G. Gao and G. Lachapelle, "A novel architecture for ultra-tight HSGPS-INS integration," *J. Global Position. Syst*, vol. 7, no. 1, pp. 46–61, Jan. 2008. [Online]. Available: http://www.scirp.org/journal/PaperInformation.aspx?paperID=381

[13] G. Falco, M. Nicola, and M. Pini, "Positioning based on tightly coupled multiple sensors: A practical implementation and experimental assessment," *IEEE Access*, vol. 6, pp. 13101–13116, 2018.

[14] J. Elfring, E. Torta, and R. van de Molengraft, "Particle filters: A hands-on tutorial," *Sensors*, vol. 21, no. 2, p. 438, Jan. 2021. [Online]. Available: https://www.mdpi.com/1424-8220/21/2/438

[15] M. Caceres Duran, P. Closas, E. Falletti, C. Fernández-Prades, M. Nájar, and F. Sottile, "Signal processing for hybridization," in *Satellite and Terrestrial Radio Positioning Technique*, D. Dardari, E. Falletti, and M. Luise, Eds. Oxford, U.K.: Academic, 2012, ch. 6, pp. 317–382, doi: 10.1016/B978-0-12-382084-6.00006-4.

[16] M. S. Arulampalam, S. Maskell, N. Gordon, and T. Clapp, "A tutorial on particle filters for online nonlinear/non-Gaussian Bayesian tracking," *IEEE Trans. Signal Process.*, vol. 50, no. 2, pp. 174–188, Feb. 2002, doi: 10.1109/78.978374.

[17] A. Minetto, A. Gurrieri, and F. Dovis, "A cognitive particle filter for collaborative DGNSS positioning," *IEEE Access*, vol. 8, pp. 194765–194779, 2020.

[18] J. Georgy, A. Noureldin, and C. Goodall, "Vehicle navigator using a mixture particle filter for inertial sensors/odometer/map data/GPS integration," *IEEE Trans. Consum. Electron.*, vol. 58, no. 2, pp. 544–552, May 2012.

[19] H. Zhou, Z. Yao, C. Fan, S. Wang, and M. Lu, "Rao-Blackwellised particle filtering for low-cost encoder/INS/GNSS integrated vehicle navigation with wheel slipping," *IET Radar, Sonar Navigat.*, vol. 13, no. 11, pp. 1890–1898, Nov. 2019. [Online]. Available: https://ietresearch.onlinelibrary.wiley.com/doi/abs/10.1049/iet-rsn.2019.0108

[20] J. Georgy, A. Noureldin, M. J. Korenberg, and M. M. Bayoumi, "Low-cost three-dimensional navigation solution for RISS/GPS integration using mixture particle filter," *IEEE Trans. Veh. Technol*, vol. 59, no. 2, pp. 599–615, Feb. 2010.

[21] R. van der Merwe, A. Doucet, N. de Freitas, and E. Wan, "The unscented particle filter," Eng. Dept., Cambridge Univ., Cambridge, U.K., Tech. Rep. CUED/F-INFENG/TR 380, 2001.

[22] C. Kim, R. Sakthivel, and W. K. Chung, "Unscented FastSLAM: A robust and efficient solution to the SLAM problem," *IEEE Trans. Robot.*, vol. 24, no. 4, pp. 808–820, Aug. 2008.

[23] S. Julier, J. Uhlmann, and H. F. Durrant-Whyte, "A new method for the nonlinear transformation of means and covariances in filters and estimators," *IEEE Trans. Autom. Control*, vol. 45, no. 3, pp. 477–482, Mar. 2000.

[24] E.-H. Shin, "Estimation techniques for low-cost inertial navigation," Ph.D. dissertation, Dept. Geomatics Eng., Schulich School Eng., Univ. Calagary, Calgary, AB, Canada, 2005. [Online]. Available: https://prism.ucalgary.ca/handle/1880/103387

[25] Y. Meng, S. Gao, Y. Zhong, G. Hu, and A. Subic, "Covariance matching based adaptive unscented Kalman filter for direct filtering in INS/GNSS integration," *Acta Astron.*, vol. 120, pp. 171–181, Mar. 2016. [Online]. Available: https://www.sciencedirect.com/science/article/pii/S0094576515004592

[26] H. Kuusniemi, "User-level reliability and quality monitoring in satellite-based personal navigation," Ph.D. dissertation, Dept. Inf. Technol., Tampere Univ. Technol., Tampere, Finland, 2005. [Online]. Available: https://tutcris.tut.fi/portal/en/publications/usellevel-reliability-and-quality-monitoring-in-satellitebased-personal-navigation(b55448d2-0785-418a-9ccc-83aec2d47c31).html

[27] A. H. Mohamed and K. P. Schwarz, "Adaptive Kalman filtering for INS/GPS," *J. Geodesy*, vol. 73, no. 4, pp. 193–203, 1999, doi: 10.1007/s001900050236.

[28] J. Zhou, S. Knedlik, and O. Loffeld, "INS/GPS tightly-coupled integration using adaptive unscented particle filter," *J. Navigat.*, vol. 63, no. 3, pp. 491–511, Jul. 2010, doi: 10.1017/S0373463310000068.

[29] J. Wang, M. P. Stewart, and M. Tsakiri, "Adaptive Kalman filtering for integration of GPS with GLONASS and INS," in *Geodesy Beyond*, K.-P. Schwarz, Ed. Berlin, Germany: Springer, 2000, pp. 325–330.

[30] D. Gebre-Egziabher, "What is the difference between'loose','tight','ultra-tight'and'deep'integration strategies for INS and GNSS," *Inside GNSS*, vol. 2, no. 1, pp. 28–32, 2007.

[31] A. Bose, K. Bhat, and T. Kurian, "Autonomous strapdown inertial navigation," in *Fundamentals Of Navigation Inertial Sensors*. New Delhi, India: PHI Learning, Jan. 1997, ch. 2, pp. 19–73, doi: 10.1002/9781119547860.ch2.

[32] M. Grewal, L. Weill, and A. Andrews, "Fundamentals of satellite and inertial navigation," in *Global Positioning Systems, Inertial Navigation, and Integration*. Hoboken, NJ, USA: Wiley, 2007, ch. 2, pp. 18–52, doi: 10.1002/9780470099728.ch2.

[33] U. Iqbal, J. Georgy, W. F. Abdelfatah, M. J. Korenberg, and A. Noureldin, "Pseudoranges error correction in partial GPS outages for a nonlinear tightly coupled integrated system," *IEEE Trans. Intell. Transp. Syst.*, vol. 14, no. 3, pp. 1510–1525, Sep. 2013.

[34] D. Titterton and J. Weston, "Basic principles of strapdown inertial navigation systems," in *Strapdown Inertial Navigation Technology*, 2nd ed. Stevenage, U.K.: The Institution of Engineering and Technology, 2004, ch. 3, pp. 17–58, doi: 10.1049/PBRA017E.

[35] I. Skog and P. Handel, "In-car positioning and navigation technologies—A survey," *IEEE Trans. Intell. Transp. Syst.*, vol. 10, no. 1, pp. 4–21, Mar. 2009, doi: 10.1109/TITS.2008.2011712.

[36] R. E. Griffin and A. P. Sage, "Sensitivity analysis of discrete filtering and smoothing algorithms," *AIAA J.*, vol. 7, no. 10, pp. 1890–1897, Oct. 1969, doi: 10.2514/3.5477.

[37] H. Liu, S. Nassar, and N. El-Sheimy, "Two-filter smoothing for accurate INS/GPS land-vehicle navigation in urban centers," *IEEE Trans. Veh. Technol.*, vol. 59, no. 9, pp. 4256–4267, Nov. 2010.

[38] K. Li, B. Hu, L. Chang, and Y. Li, "Comparison of direct navigation mode and indirect navigation mode for integrated SINS/GPS," *Trans. Inst. Meas. Control*, vol. 38, no. 1, pp. 3–13, Jan. 2016, doi: 10.1177/0142331214568236.

[39] C. Jekeli, *Inertial Navigation Systems with Geodetic Applications*. Berlin, Germany: De Gruyter, Oct. 2012, doi: 10.1515/9783110800234.

[40] P. Misra and P. Enge, *Global Positioning System: Signals, Measurements, and Performance*, 2nd ed. Kathmandu, Nepal: Ganga-Jamuna Press, 2010. [Online]. Available: https://www.navtechgps.com/global-positioning-system-signals-measurements-and-performance-revised-second-edition-paperback/

[41] P. C. Gomez, "Bayesian signal processing techniques for GNSS receivers: From multipath mitigation to positioning," Ph.D. dissertation, Dept. Signal Theory Commun., Univ. Politecnica de Catalunya, Barcelona, Spain, Jun. 2009. [Online]. Available: https://theses.eurasip.org/theses/310/bayesian-signal-processing-techniques-for-gnss/

[42] W. Song, Z. Wang, J. Wang, F. E. Alsaadi, and J. Shan, "Distributed auxiliary particle filtering with diffusion strategy for target tracking: A dynamic event-triggered approach," *IEEE Trans. Signal Process.*, vol. 69, pp. 328–340, 2021.

[43] J. Lim, H.-S. Kim, and H.-M. Park, "Interactive-multiple-model algorithm based on minimax particle filtering," *IEEE Signal Process. Lett.*, vol. 27, pp. 36–40, 2020.

[44] W. Xia, M. Sun, and Z. Zhou, "Diffusion collaborative feedback particle filter," *IEEE Signal Process. Lett.*, vol. 27, pp. 1185–1189, 2020.

[45] J. V. Candy, *Particle-Based Bayesian State-Space Processors*. Hoboken, NJ, USA: Wiley, 2016, pp. 253–326.

[46] A. Doucet, S. Godsill, and C. Andrieu, "On sequential Monte Carlo sampling methods for Bayesian filtering," *Statist. Comput.*, vol. 10, no. 3, pp. 197–208, 2000, doi: 10.1023/A:1008935410038.

[47] N. Gordon, D. Salmond, and A. Smith, "Novel approach to nonlinear/non-Gaussian Bayesian state estimation," *IEEE Proc. F Radar Signal Process.*, vol. 140, no. 6, pp. 107–113, Apr. 1993. [Online]. Available: https://digital-library.theiet.org/content/journals/10.1049/ip-f-2.1993.0015

[48] R. Van Der Merwe and E. A. Wan, "Sigma-point Kalman filters for probabilistic inference in dynamic state-space models," Ph.D. dissertation, OGI School Sci. Eng., Oregon Health Sci. Univ., Portland, OR, USA, Apr. 2004.

[49] J. Zhou, "Low-cost MEMS-INS/GPS integration using nonlinear filtering approaches," Ph.D. dissertation, Center Sensorsyst., Univ. Siegen, Siegen, Germany, Apr. 2013. [Online]. Available: https://dspace.ub.uni-siegen.de/handle/ubsi/750

[50] A. Dhital, J. Bancroft, and G. Lachapelle, "A new approach for improving reliability of personal navigation devices under harsh GNSS signal conditions," *Sensors*, vol. 13, no. 11, pp. 15221–15241, Nov. 2013. [Online]. Available: https://www.mdpi.com/1424-8220/13/11/15221

[51] L. Zheng, H. Zhang, Z. Qifan, and H. Che, "An adaptive low-cost INS/GNSS tightly-coupled integration architecture based on redundant measurement noise covariance estimation," *Sensors*, vol. 17, no. 9, Oct. 2017. [Online]. Available: https://www.mdpi.com/1424-8220/17/9/2032
[52] Q. Zhou, H. Zhang, Y. Li, and Z. Li, "An adaptive low-cost GNSS/MEMS-IMU tightly-coupled integration system with aiding measurement in a GNSS signal-challenged environment," *Sensors*, vol. 15, no. 9, pp. 23953–23982, Sep. 2015. [Online]. Available: https://www.mdpi.com/1424-8220/15/9/23953
[53] P. Savage, "Strapdown inertial navigation integration algorithm design Part 1: Attitude algorithms," *J. Guid., Control Dyn.*, vol. 21, no. 1, pp. 19–28, 1998.
[54] P. G. Savage, "Strapdown inertial navigation integration algorithm design Part 2: Velocity and position algorithms," *J. Guid., Control, Dyn.*, vol. 21, no. 2, pp. 208–221, 1998.
[55] T. B. Schön, F. Gustafsson, and P.-J. Nordlund, "Marginalized particle filters for mixed linear/nonlinear state-space models," *IEEE Trans. Signal Process.*, vol. 53, no. 7, pp. 2279–2289, Jul. 2005.
[56] P. Closas and M. F. Bugallo, "Improving accuracy by iterated multiple particle filtering," *IEEE Signal Process. Lett.*, vol. 19, no. 8, pp. 531–534, Aug. 2012.

OLIVIERO VOUCH (Member, IEEE) was born in Casale Monferrato, Italy, in 1996. He received the B.Sc. degree in electronics and communications engineering (ECE) and the M.Sc. degree in communications and computer networks engineering (CCNE) from the Politecnico di Torino, Turin, Italy, in 2018 and 2020, respectively, where he is currently pursuing the Ph.D. degree with the Department of Electronics and Telecommunications (DET). He is also a member of the Navigation Signal Analysis and Simulation (NavSAS) Research Group. His academic background includes advanced signal processing. His current research interest includes advanced Bayesian estimation applied to navigation sensors integration.

ALEX MINETTO (Member, IEEE) was born in Pinerolo, Italy, in 1990. He received the B.Sc. and M.Sc. degrees in telecommunications engineering from the Politecnico di Torino, Turin, Italy, and the Ph.D. degree in electrical, electronics and communications engineering, in 2020. He joined the Department of Electronics and Telecommunications, Politecnico di Torino, as a Research and Teaching Assistant, in 2019. He spent a six-month internship at European Organisation for the Exploitation of Metereological Satellites (EUMETSAT), Darmstadt, Germany, in 2015. His current research interests include signal processing and advanced Bayesian estimation applied to global navigation satellite system (GNSS) cooperative receivers.

GIANLUCA FALCO was born in Cuneo, Italy, in 1981. He received the M.Sc. and Ph.D. degrees in electronics and communication engineering from the Politecnico di Torino, Turin, Italy, in 2007 and 2011, respectively. From May 2009 to March 2010, he was a Visiting Student at the Queensland Centre for Advanced Technologies (QCAT), Brisbane, QLD, Australia. Since 2011, he has been a Communication Engineer with the Space and Navigation Technologies Research Area, LINKS Foundation, Turin. His research interests include multisensors fusion, particularly between GNSS and inertial navigation systems, as well as on advanced processing techniques for dual-frequency and multi-constellation GNSS receivers.

FABIO DOVIS (Member, IEEE) was born in Bruino, Italy, in 1970. He received the M.Sc. and Ph.D. degrees from the Politecnico di Torino, Turin, Italy, in 1996 and 2000, respectively. He joined the Department of Electronics and Telecommunications, Politecnico di Torino, as an Assistant Professor, in 2004. Since 2014, he has been an Associate Professor Department of Electronics and Telecommunications, Politecnico di Torino, where he coordinates the Navigation Signal Analysis and Simulation (NavSAS) Research Group. He has a relevant experience in European projects in satellite navigation as well as cooperation with industries and research institutions. His research interests include the design of GPS and Galileo receivers and advanced signal processing for interference and multipath detection and mitigation, as well as ionospheric monitoring. He serves as a member of the IEEE Aerospace and Electronics Systems Society Navigation Systems Panel.